Supporting Information for "The impact of recent climate change on the global ocean carbon sink"

Frauke Bunsen[1], Cara Nissen[1,2], Judith Hauck[1]

[1]Alfred Wegener Institute Helmholtz Centre for Polar and Marine Research, Bremerhaven, Germany

[2]Department of Atmospheric and Oceanic Sciences and Institute of Arctic and Alpine Research, University of Colorado, Boulder, Boulder, CO, USA

Contents of this file

1. Texts S1 to S7
2. Figures S1 to S9
3. Table S1 to S2

Corresponding author: Frauke Bunsen, Marine Biogeosciences, Alfred Wegener Institute Helmholtz Centre for Polar and Marine Research, Am Handelshafen 12, 27570 Bremerhaven, Germany. (frauke.bunsen@awi.de)

February 21, 2024, 11:13pm

In this supplementary material, we provide more detail on our methods and the results:

Text S1: Description of the ocean biogeochemical model used in this study

Text S2: Extended description of the online assessment method

Text S3 & S4: Extended description of the offline assessment method

Text S5: Comparison of direct and indirect wind effects

Text S6: Description of the results of the offline analysis

Text S7: Description of the effect of climate on the North Pacific CO_2 flux

Fig. S1: Simulated evolution of the global mean sea surface temperature without global warming

Fig. S2: Global distribution of the wind effect on the CO_2-flux trend (estimated offline)

Fig. S3: Effects of different drivers on the global CO_2 flux 2000-2019 and its trend 1968-2019 (estimated offline)

Fig. S4: Ocean-borne fraction of CO_2 emissions

Fig. S5: Global map of the effects of rising atmospheric CO_2 and climate change on the mean CO_2 flux 2000-2019 obtained as the difference between two simulations

Fig. S6: Contributions of biomes to the globally integrated wind-driven and warming-driven CO_2-flux trend, including biome definition

Fig. S7: Local climate effect on the CO_2 flux and its drivers (MLD, NPP, SIC) for the North Pacific

Fig. S8: Local climate effect on the CO_2 flux for the (sub)tropics

Fig. S9: Local climate effect on the CO_2 flux and its drivers (MLD, NPP, SIC) in the Southern Ocean

Table S1: Summary of model simulations A-F

Table S2: Global CO_2 fluxes (temporal mean and trend) over time periods directly comparable to previous studies

Text S1: Ocean biogeochemical model

We use the Finite Element Sea-ice Ocean Model (FESOM) version 1.4 (an updated and improved version of the release described in Wang et al., 2014) coupled with the biogeochemical model REcoM2 (Hauck et al., 2013, Schourup-Kristensen et al., 2014). FESOM1.4 is a global general ocean circulation and sea-ice model. FESOM1.4 provides a flexible multi-resolution modelling functionality through an unstructured mesh approach. Here, we use the CORE mesh (126859 surface nodes), roughly corresponding to a resolution of 1°x1° with increased resolution in equatorial and polar regions, and consisting of 46 vertical layers, with a thickness of 5 meters near the surface and progressively increasing thickness with depth.

REcoM2 is an ocean biogeochemistry and ecosystem model with state-of-the-art complexity at the time of writing, i.e. comparable to other models used in the framework of the Global Carbon Budget or RECCAP (REgional Carbon Cycle Assessment and Processes, `https://www.globalcarbonproject.org/reccap/`). In the version used here, REcoM2 has two phytoplankton functional groups (diatoms and small calcifying phytoplankton),

one zooplankton functional group and one class of sinking detritus. REcoM2 simulates the oceanic cycle of carbon, including calcium carbonate, oxygen and the nutrients nitrogen, silicon and iron. The carbonate chemistry and ocean-air fluxes are calculated with mocsy 2.0 (Orr and Epitalon, 2015) following the protocol of the Ocean Carbon Model Intercomparison Project (Orr et al., 2017). A documentation of REcoM2 is available online (`https://recom.readthedocs.io/en/latest/index.html`, Gürses (2021)), and the model equations are published in the supplements of Hauck et al. (2013). FESOM1.4-REcoM2 has been evaluated in Hauck et al. (2020) with respect to the oceanic carbon cycle, showing reasonable agreement with other global ocean biogeochemical models and with surface ocean pCO_2 observations.

Text S2: Extended description of the online assessment method

By comparing the CO_2 flux in different model simulations, we quantify the impact of the following variables on the flux: Atmospheric CO_2, winds, warming and the combined effect of all physical climate variability. Additionally, a spurious flux (bias) of natural carbon and its trend (drift) arise at repeat-year climate forcing and constant atmospheric CO_2. Model drift and the preindustrial CO_2 flux are quantified with the control simulation (B, Table S1):

$$\text{bias and drift} = \text{B} \tag{1}$$

The effect of rising atmospheric CO_2 alone ($atmCO_2$) is calculated from simulations C and B:

$$atmCO_2 = C - B \tag{2}$$

The effect of climate (clim) on the total CO_2 flux is calculated from the difference between the historical simulation (A) and simulation C:

$$clim_{total} = A - C \tag{3}$$

The effect of climate on the natural CO_2 flux (nat) is calculated from the control simulation (B) and the simulation with historically varying climate at preindustrial atmospheric CO_2 (D):

$$clim_{nat} = D - B \tag{4}$$

Consequently, the effect of climate on the flux of anthropogenic CO_2 (ant) is the difference between these two terms:

$$clim_{ant} = \underbrace{(A - C)}_{total} - \underbrace{(D - B)}_{nat} \tag{5}$$

The effects of warming and winds on the total CO_2 flux are calculated as the difference between the historical simulation A and the simulations E or F:

$$warming = A - E \tag{6}$$

$$winds = A - F \tag{7}$$

Finally, the residual, that is the fraction of the climate-induced change in the historical CO_2 flux that cannot be explained by wind and temperature effects, is attributed to precipitation, atmospheric pressure and nonlinearities arising from the simultaneous change

in multiple atmospheric forcings:

$$\text{residual} = \underbrace{(\text{A} - \text{C})}_{\text{full climate}} - \underbrace{(\text{A} - \text{E})}_{\text{warming}} - \underbrace{(\text{A} - \text{F})}_{\text{winds}} \tag{8}$$

Text S3: Extended description of the offline assessment method. Part 1: The impact of winds, SST, SIC, sAlk, sDIC and salinity and freshwater fluxes on the CO_2 flux

We approximate the impact of the following variables (X_i) on the CO_2 flux offline from monthly mean model output: wind velocity, sea surface temperature (SST), sea-ice concentration (SIC), salinity-normalized alkalinity (sAlk), salinity and freshwater fluxes (S+FW) and salinity-normalized DIC (sDIC). Following Lovenduski et al. (2007), we derive the sensitivity of the CO_2 flux to changes in the respective variables analytically. The analytic approximations are based on the model equation for the CO_2 flux (F_{surf}), which is calculated following the protocol of Orr et al., (2015) as:

$$F = \alpha k_w \cdot \Delta\text{pCO}_2 \tag{9}$$

where ΔpCO_2 is the difference of atmospheric ($^{\text{A}}$) and oceanic ($^{\text{O}}$) partial pressures ($\text{pCO}_2^{\text{A}} - \text{pCO}_2^{\text{O}}$), k_w is the gas transfer velocity (piston velocity) which depends on wind speed and sea-ice concentration, and α is the solubility of CO_2 in seawater which depends on temperature and salinity. Further, the partial pressure of CO_2 in water (pCO_2^{O}) is a function of dissolved inorganic carbon (DIC), alkalinity (Alk), temperature and salinity (Sarmiento and Gruber, 2006).

Following Lovenduski et al. (2007), the contribution of each variable X_i to the change in the CO_2 flux is linearly approximated. Originally, Lovenduski et al. (2007) used this

approach to approximate the difference in the CO_2 flux between a positive phase of the Southern Annular Mode and the mean state. Conceptually, the method can be used to estimate the impact of changes in the variables on the CO_2 flux on any time scale. Here, the offline analysis is applied to (1) the mean air-sea CO_2 flux 2000-2019 relative to 1960-1979 and (2) the trend in the air-sea CO_2 flux 1958-2019.

To quantify the climate-related effect of each variable on the CO_2 flux, we use the simulation with variable climate at preindustrial CO_2 (D) to exclude variability in sDIC, pCO_2^O and the CO_2 flux originating from the increase in atmospheric CO_2. Here, we capitalize on the fact that the climate effect is dominated by natural CO_2 fluxes as the natural ocean carbon pool exceeds the anthropogenic pool by far (Wanninkhof et al, 2013).

The contribution of each variable to the trend 1958-2019 (mean 2000-20019) of the CO_2 flux (β_F) is approximated by calculating the trend 1958-2019 (mean 2000-2019) in the respective variable (β_{X_i}) and the sensitivity of the CO_2 flux to changes in that variable:

$$\beta_F \approx \sum_i \left[\frac{\partial F}{\partial X_i}\right] \beta_{X_i} \tag{10}$$

where square brackets denote the [**temporal mean**] averaged over the whole time series (1958-2019) at each grid point, $\frac{\partial F}{\partial X_i}$ is the sensitivity to the variable derived from analytical expressions and calculated with values from the model output at every grid point, and β_{X_i} is the trend 1958-2019 (mean 2000-20019) of the variable at each grid point.

Note:

- Squared wind velocities: Because of the quadratic dependency of the piston velocity k_w on the wind velocity, we relate the trend 1958-2019 (mean 2000-20019) of the CO_2 flux to the trend 1958-2019 (mean 2000-20019) of squared wind velocities.

• Seasonality of sea-ice: Because of the high seasonality of sea-ice concentration, we calculate the sensitivity and trend 1958-2019 (mean 2000-20019) for sea-ice after grouping the data by month-of-the-year.

• Salinity-normalization: Changes in surface DIC (Alk) can occur through multiple processes, namely by biological processes, advective transport and mixing, surface fluxes of CO_2 and through freshwater fluxes. Freshwater from precipitation has low DIC (Alk), so that adding freshwater to the ocean mostly decreases surface ocean DIC (Alk), whereas removing freshwater through evaporation increases DIC (Alk) (Sarmiento and Gruber, 2006). To eliminate the effect of freshwater fluxes from the DIC (Alk) trend 1958-2019 (mean 2000-20019), we use sea surface salinity as a tracer for freshwater fluxes and normalize DIC (Alk) by salinity. At each grid point, DIC (Alk) is normalized by the local time-mean sea surface salinity.

Text S4: Extended description of the offline assessment method. Part 2: The impact of biology, surface flux and circulation on sDIC

In an additional step, the trend of sDIC (1958-2019) is attributed to either changes in (1) biological export, (2) air-sea CO_2 fluxes or (3) circulation, advection and mixing (calculated as the residual). They can be estimated following Lovenduski et al. (2007):

$$\frac{d(\mathrm{sDIC})}{dt} = J_{\mathrm{bio}} + J_{\mathrm{surf}} + J_{\mathrm{circ}} \tag{11}$$

where t is time, sDIC is salinity-normalized surface DIC, J_{bio} is the loss of mixed-layer sDIC by export production, J_{surf} is the rate of change caused by the air-sea flux of CO_2 and J_{circ} relates to the transport of sDIC with ocean circulation, advection and mixing.

sDIC is assumed to be uniform throughout depth within the mixed layer, and for simplicity, surface values of sDIC are used for the calculations. Thereby, J_{bio}, J_{surf} and J_{circ} describe the temporal change of sDIC at the surface and throughout the mixed layer. Hence, J_{bio}, J_{surf} and J_{circ} have units of per volume (of mixed layer water; like sDIC) and per time.

To calculate J_{bio}, we use the detritus concentration at the bottom of the mixed layer (MLD), defined by a density-threshold criterion ($0.03\,\mathrm{kg\,m^{-3}}$). In our model, detritus carbon exists in the form of particulate organic carbon and $CaCO_3$. The particles have a vertical sinking velocity; unlike dissolved carbon which only follows the circulation. To get the average daily flux of detritus through the base of the mixed layer from the detritus concentration, the detritus concentration is multiplied with the sinking velocity v_{detritus} at the base of the mixed layer, which is $v_{\mathrm{detritus}} = 0.0288\,\mathrm{d^{-1}} \cdot \mathrm{MLD} + 20\,\mathrm{m\,d^{-1}}$. The flux of detritus through the base of the mixed layer is then divided by the climatological depth of the mixed layer (i.e. the MLD averaged from 1958-2019 for each month of the year) to obtain J_{bio} in units of $\mathrm{mmol\,C\,m^{-3}\,d^{-1}}$.

Analogously, J_{surf} is the air-sea flux of CO_2 divided by the climatological depth of the mixed layer. To obtain J_{surf} and J_{bio}, we divide by the climatological mixed layer depth rather than the monthly MLD in order to remove the effect of interannual MLD variations on J_{surf} and J_{bio}. The change in the sDIC concentration that occurs through the dispersion of detritus losses and surface carbon fluxes over an interannually variable mixed layer depth is thus attributed to the circulation term.

Here, we go beyond the analysis of Lovenduski et al. (2007) by estimating the trend in sDIC due to the surface flux, the export flux and the circulation [mmol C m^{-3}perdecade(dec)] from the trend in the sDIC tendencies [mmol C m^{-3} d^{-1} dec^{-1}] through integration. We apply this latter analysis to simulation A, B, C and D to separately quantify the effect of both atmospheric CO_2 and climate on the trends.

Text S5: Comparison of direct and indirect wind effects

The simulated wind effect on the global CO_2 flux trend 1958-2019 is larger (2.9×10^{-2} PgC yr^{-1} dec^{-1}) than the offline estimate of the wind-velocity effect on the gas transfer velocity (-1.0×10^{-2} PgC yr^{-1} dec^{-1}). While the geographic pattern of the direct effect reflects local wind changes, patterns of the simulated effect are more complex to interpret (Figures 3e and S2). Overall, indirect effects dominate the response to wind forcing through circulation changes that the offline approach fails to capture.

Text S6: Extended results of the offline analysis

In simulation D, changes in SST, winds, sAlk, sDIC and salinity and freshwater fluxes (S+FW) contribute to the climate effects on the CO_2 flux. The net climate-induced change of the globally integrated natural air-sea CO_2 flux 2000-2019 amounts to an outgassing of 0.16 PgC yr^{-1} in simulation D. According to the offline approach, the increase in SST dominates this flux change, generating an outgassing of 0.66 PgC yr^{-1} (Figure S3). However, most of the temperature effect is offset by the effects of sAlk (-0.29 PgC yr^{-1}) and

sDIC ($-0.27\,\mathrm{PgC\,yr^{-1}}$). Changes in salinity, freshwater fluxes and sea-ice concentrations have small effects globally ($< 0.05\,\mathrm{PgC\,yr^{-1}}$). Ideally, the sum of all offline decomposed climate drivers should be equal to the simulated net CO_2 flux in simulation D. However, the sum is different from the net CO_2 flux by $-0.06\,\mathrm{PgC\,yr^{-1}}$, which we attribute to the assumptions underlying the analysis. Yet, this error is small compared to the magnitude of the dominant drivers.

Text S7: Effect of climate change on the North Pacific CO_2 flux

The North Pacific is exposed to regional climate change that, in total, promotes slightly more oceanic CO_2 uptake ($5.8 \times 10^{-1}\,\mathrm{TgC\,yr^{-1}\,dec^{-1}}$ stemming from the North Pacific Subtropical Seasonally Stratified (STSS), Subpolar Seasonally Stratified (SPSS) and Ice (ICE) biomes collectively). The reasons for this are twofold: firstly, the intensification of westerly winds, mixed layer deepening and increasing net primary productivity (NPP) in the western North Pacific lead to more CO_2 uptake (Figure S7, region 1). Some observational evidence for wind-driven mixed-layer deepening (1960-2007) in region 1 and, albeit less prominent, mixed-layer shoaling in region 3 exists (Carton et al., 2008). Secondly, the retreat of sea-ice due to warming drives increased CO_2 uptake and increased NPP in the Sea of Okhotsk and in the Arctic Ocean (Figure S7, regions 2a and 2b) - although the impact is smaller than in the North Atlantic. In contrast, weaker winds lead to less CO_2 uptake in the eastern North Pacific, which is driven by decreased NPP in that area (Figure S7, region 3).

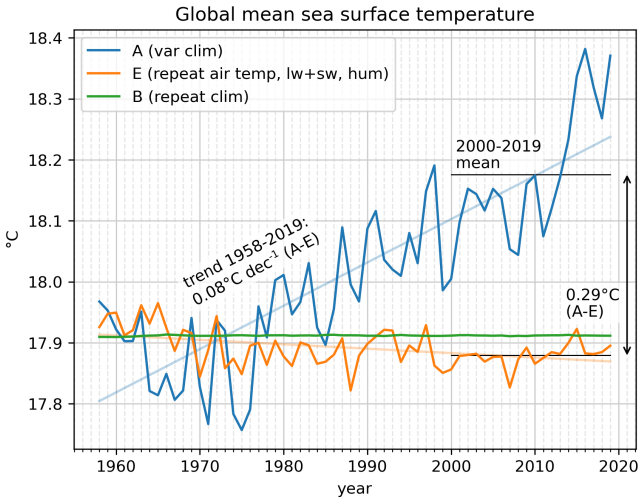

Figure S1: Global mean sea surface temperature in the historical simulation (simulation A), in the simulation with annually repeated climate forcing (simulation B) and in the simulation at the notional absence of global warming, while still allowing some climate variables to vary as in historical records (simulation E).

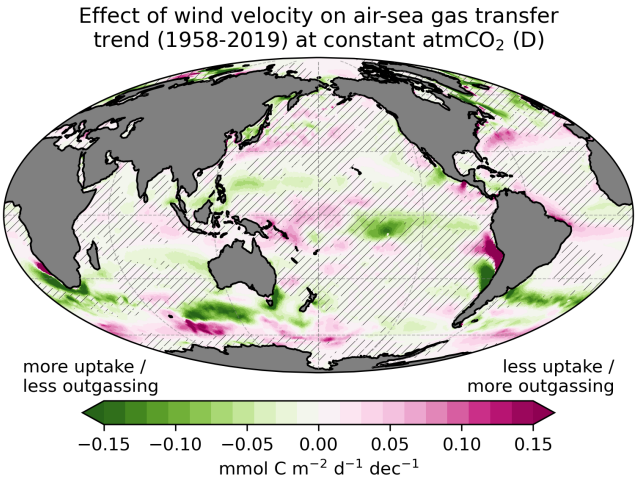

Figure S2: Offline estimate of the trend 1958-2019 in the air-sea CO_2 flux density derived from the trend of the squared wind velocity. Hatched areas indicate a low significance of the trend (p-value > 0.05). Positive values denote a trend towards more oceanic outgassing or less oceanic uptake, respectively.

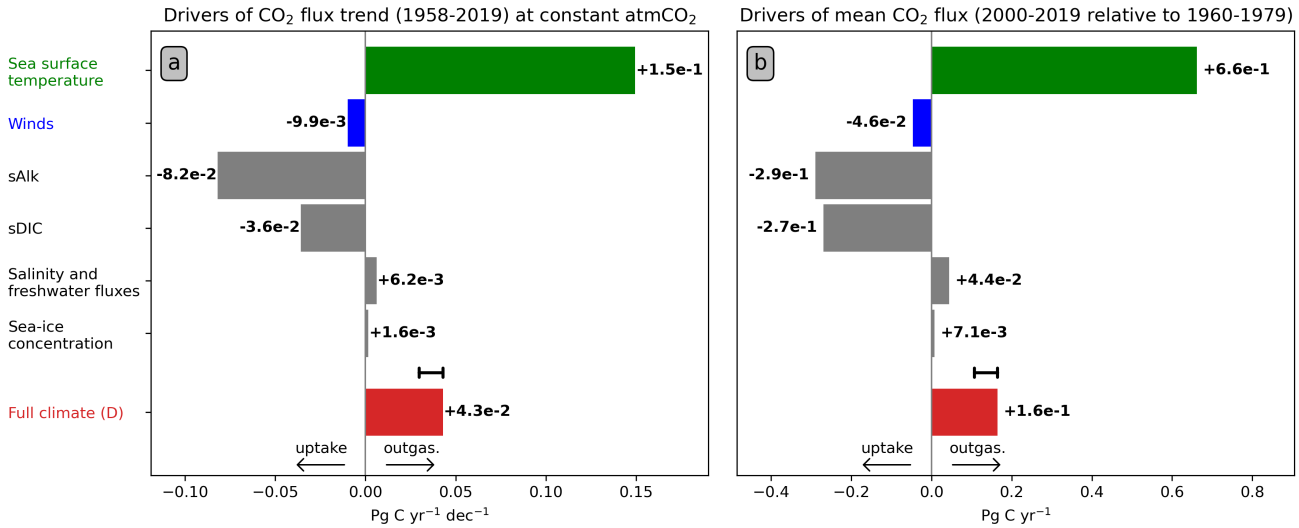

Figure S3: (a) The climate effect on the trend of the global air-sea flux of natural CO_2 (simulation D) from 1958-2019 based on an offline estimate (see Text S2). The difference ($1.3 \times 10^{-2}\,\mathrm{PgC\,yr^{-1}\,dec^{-1}}$) between the sum of all offline decomposed factors ($3.0 \times 10^{-2}\,\mathrm{PgC\,yr^{-1}\,dec^{-1}}$) and the simulated total climate effect ($4.3 \times 10^{-2}\,\mathrm{PgC\,yr^{-1}\,dec^{-1}}$) is indicated with a black symbol. (b) Like (a), but for the mean CO_2 flux 2000-2019 relative to 1960-1979.

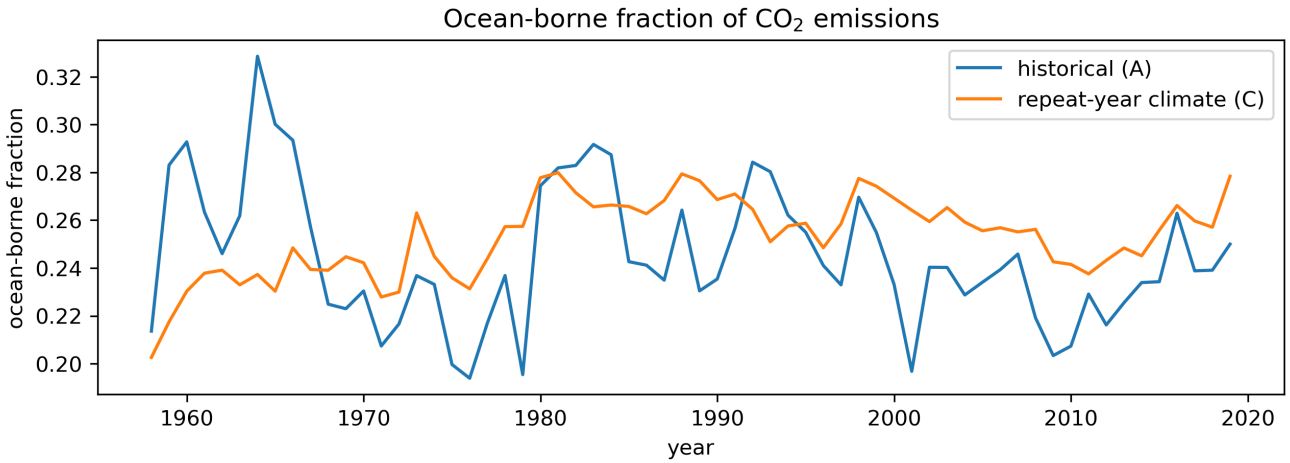

Figure S4: The ocean-borne fraction of annual CO_2 emissions in the historical simulation (A) and in the simulation with annually repeated climate forcing (C). Data for the total anthropogenic CO_2 emissions stems from the Global Carbon Budget (Friedlingstein et al., 2023).

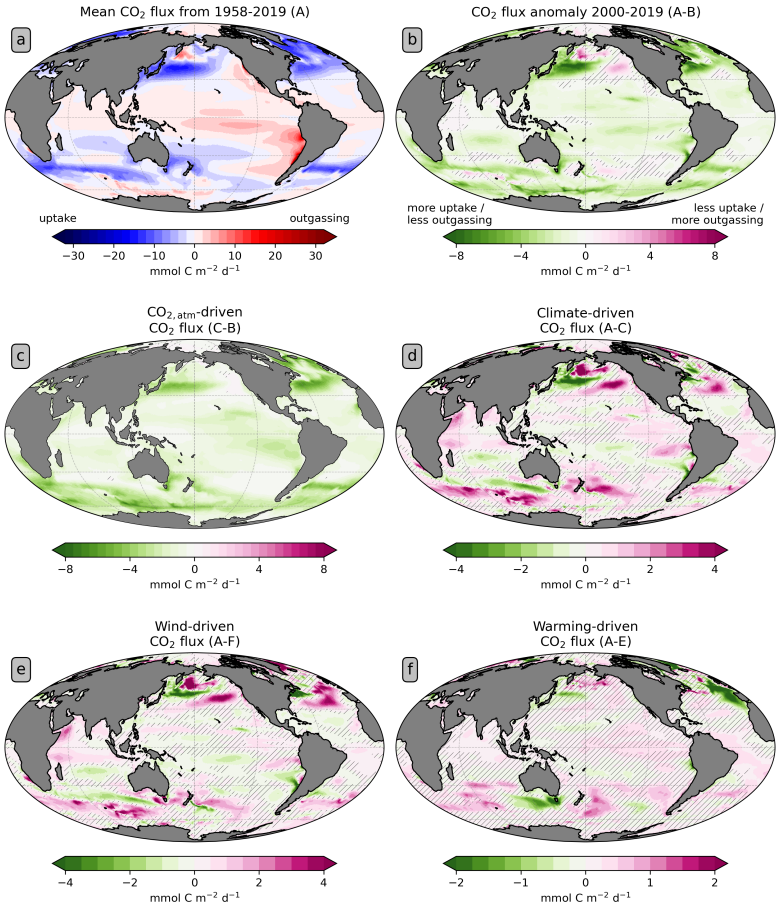

Figure S5: (a) The mean air-sea CO_2 flux density 1958-2019 and (b) the net anomaly in the CO_2 flux density 2000-2019 in the historical simulation A compared to simulation B. (c-f) The effects of the rising atmospheric CO_2 concentration and climate change on the mean CO_2 flux density 2000-2019 obtained as the difference between two simulations with and without interannual variability and trends in the respective variable(s): (c) Atmospheric CO_2 concentration, (d) full climate variability and trends, (e) winds and (f) global warming. Positive values denote more oceanic outgassing or less oceanic uptake, respectively. Hatched areas in (b-f) indicate a low significance of the difference between the two respective fields (p-value >0.05 applying a two-sided Welch's t-test).

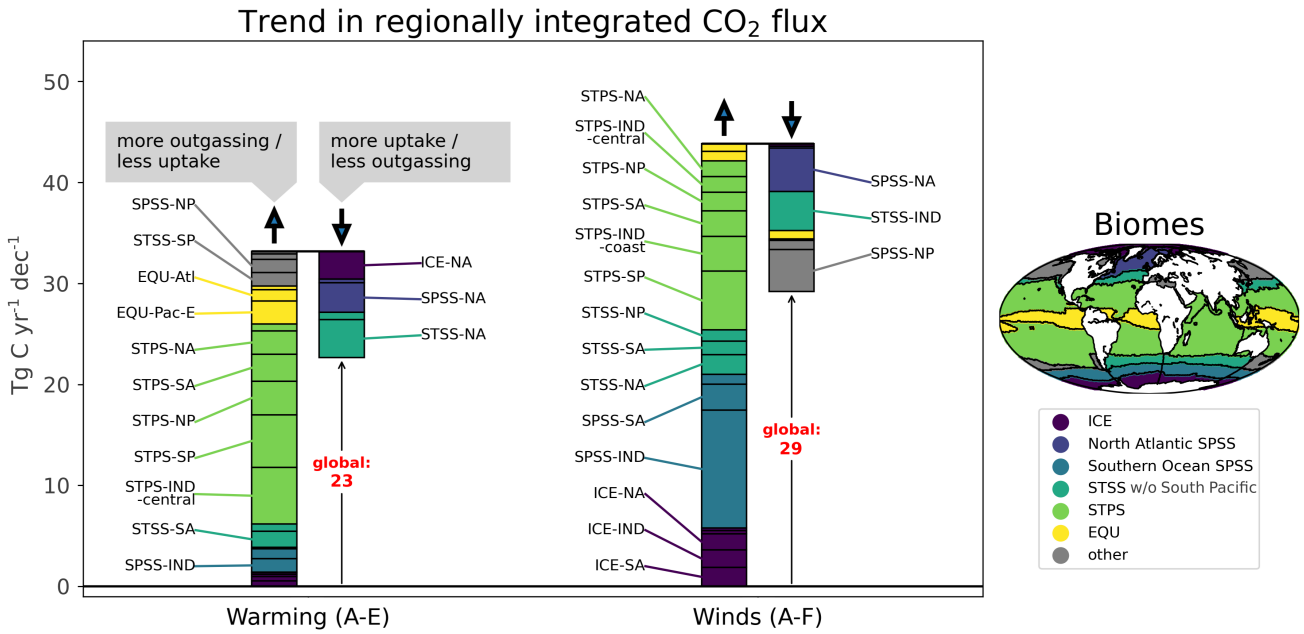

Figure S6: Regional contributions to the spatially integrated CO_2 flux trend (1958-2019) caused by winds and global warming. Biomes considered are: Ice biome (ICE), Subpolar Seasonally Stratified biome (SPSS), Subtropical Seasonally Stratified biome (STSS), Subtropical Permanently Stratified biome (STPS) and Equatorial biome (EQU) with subregions: North Atlantic (NA), North Pacific (NP), South Atlantic (SA), South Pacific (SP) and Indian Ocean (IND) (Fay and McKinley, 2014). Labels skipped for absolute contributions less than 1 TgC yr^{-1} dec^{-1}.

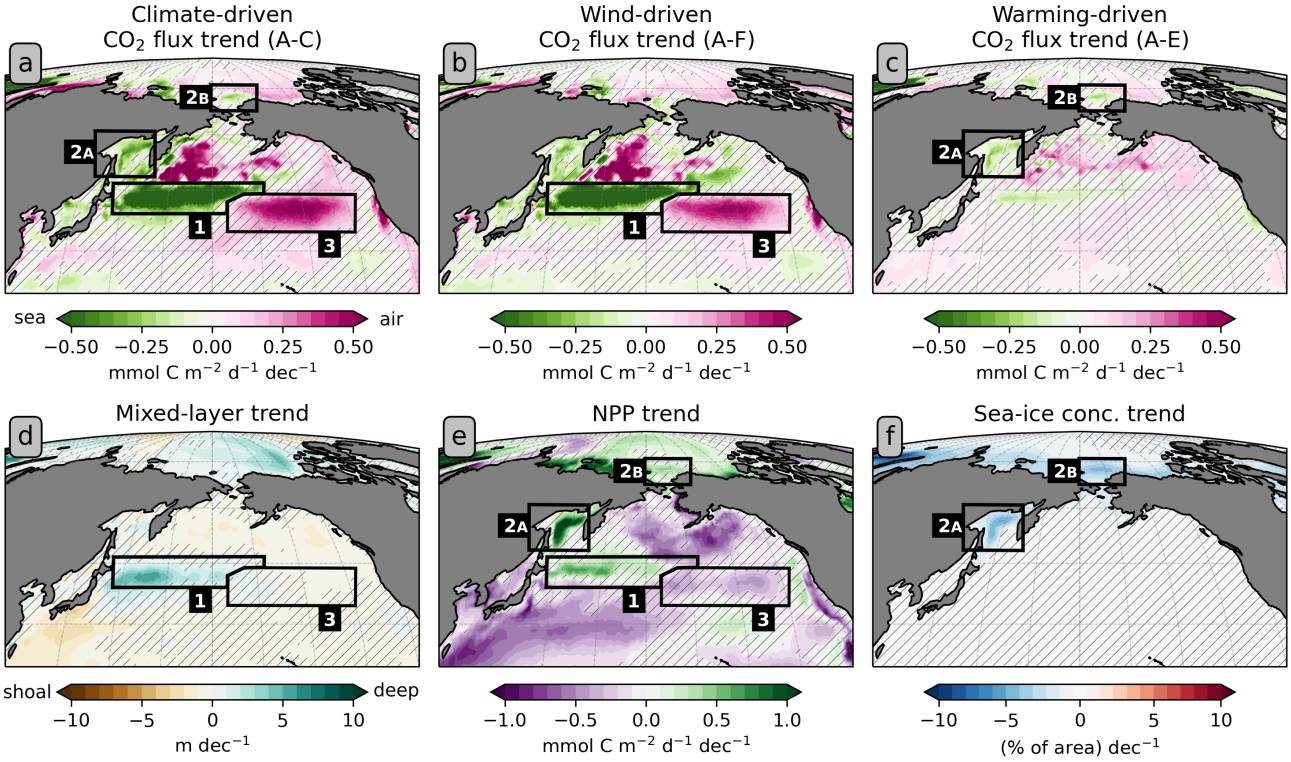

Figure S7: (a-c) North Pacific trends in the CO_2 flux density between 1958-2019 due to (a) net climate effects, (b) winds and (c) global warming. (d-f) Trends in (d) mixed layer depth, (e) NPP and (f) sea-ice concentration. Hatched areas in indicate a low significance of the trend (p-values > 0.05).

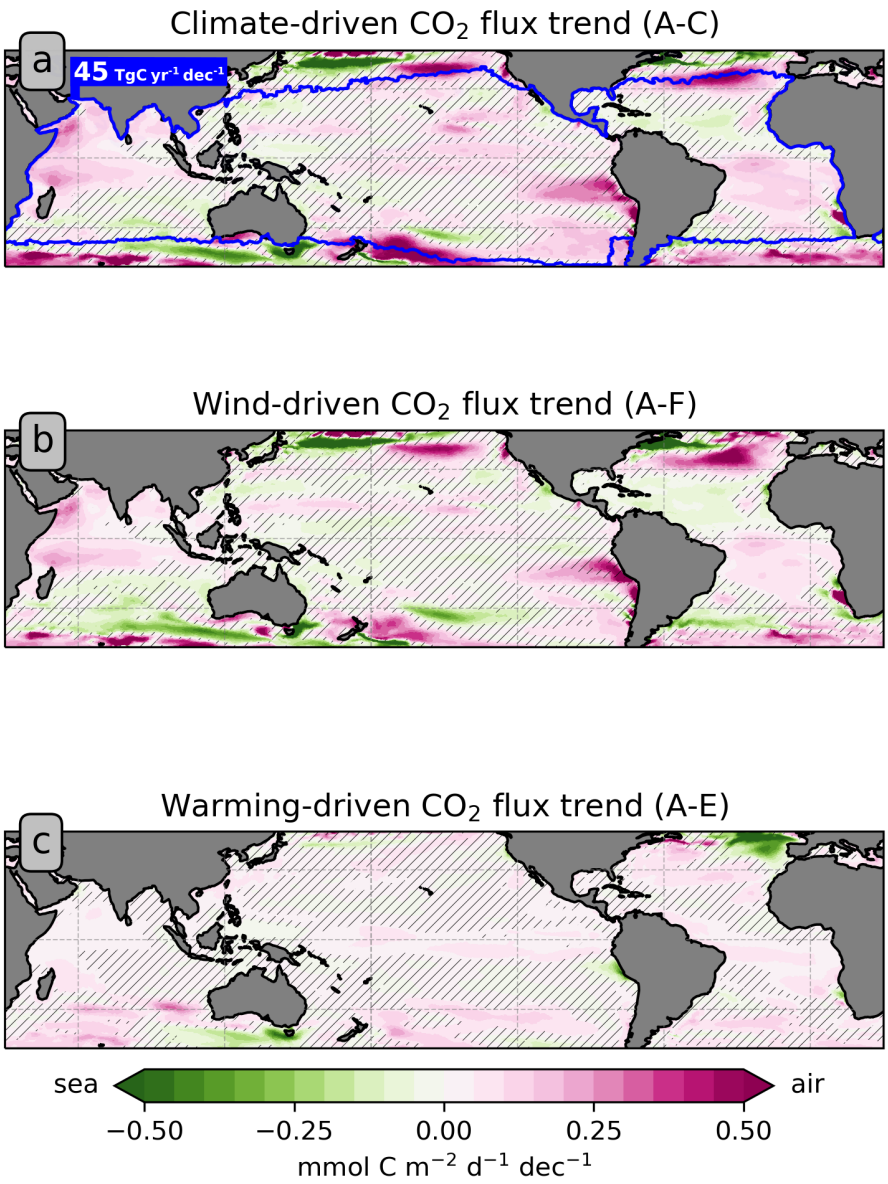

Figure S8: Trends in the CO_2 flux density between 1958-2019 in the tropics and subtropics due to (a) net climate effects, (b) winds and (c) global warming. Hatched areas in indicate a low significance of the trend (p-values > 0.05). The blue framed area follows biome definition by Fay and McKinley, 2014.

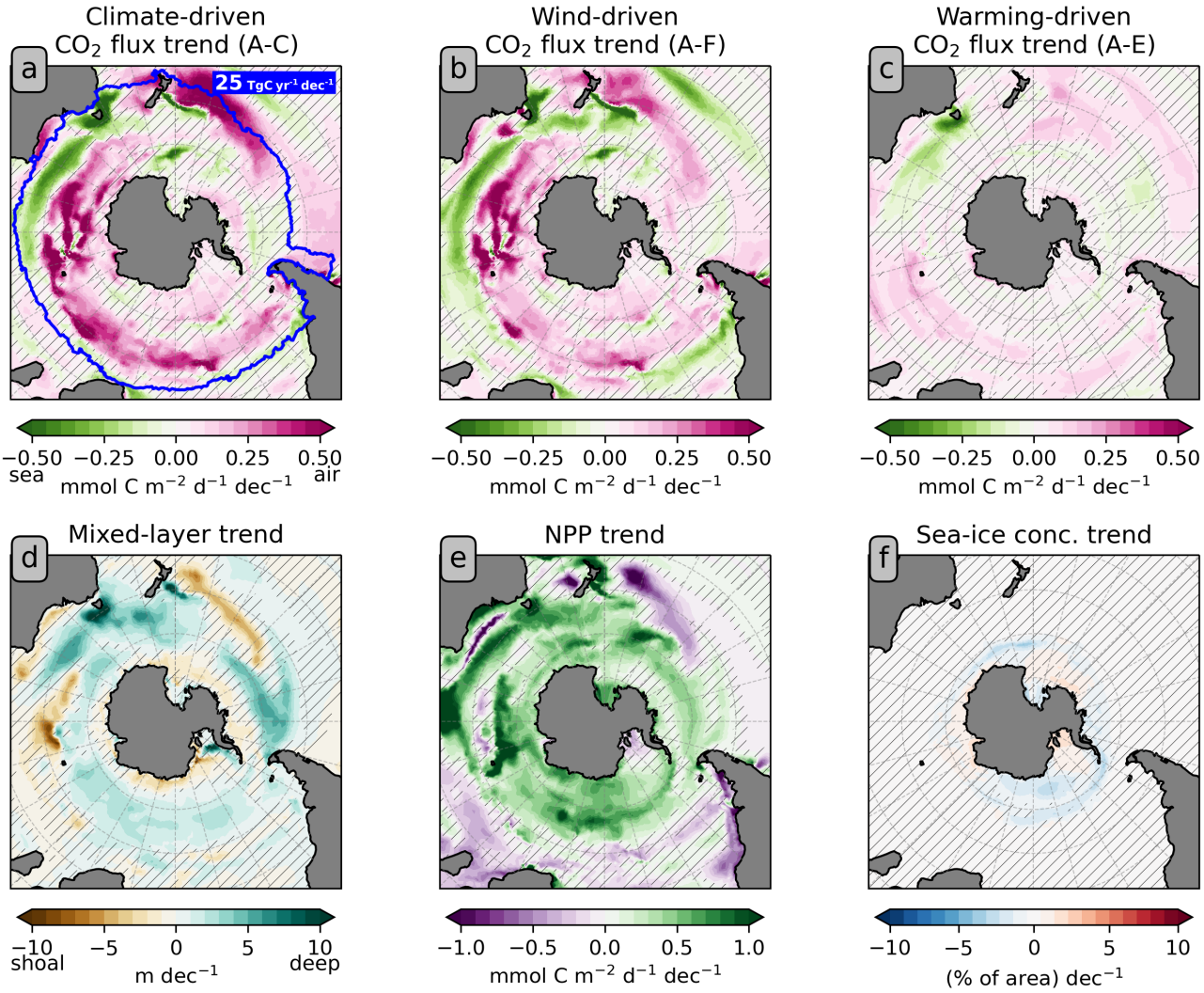

Figure S9: (a-c) Southern Ocean trends in the CO_2 flux density between 1958-2019 due to (a) net climate effects, (b) winds and (c) global warming. (d-f) Trends in (d) mixed layer depth, (e) NPP and (f) sea-ice concentration. Hatched areas in indicate a low significance of the trend (p-values > 0.05). The blue framed area follows biome definition by Fay and McKinley, 2014.

Table S1: Summary of model simulations. The forcing variables which are varying over time are denoted by 'x' for each simulation; all other variables are held constant or applied as annually repeating forcing ('-').

		A	B	C	D	E	F
atmospheric CO_2		×	-	×	-	×	×
climate	warming	×	-	-	×	-	×
	winds					×	-
	other					×	×

×: varying, -: constant/repeat-year

Table S2: Global time-mean CO_2 flux in PgC yr^{-1} and trend in PgC yr^{-1} dec^{-1} compared to the estimates of LeQuéré et al. (2010), referred to as 'LQ', and Gruber et al. (2019), referred to as 'G', over the available time periods. Furthermore, the mean CO_2 flux 2010-2019 and trend 1958-2019 are compared to the multi-model mean, minimum and maximum estimates of 10 global ocean biogeochemistry models participating in the Global Carbon Budget (Friedlingstein et al., 2023), referred to as 'GCB'. The GCB models are: NEMO3.6-PISCESv2-gas (CNRM) (Berthet et al., 2019 and Séférian et al., 2019), FESOM-2.1–REcoM2 (Gürses et al., 2023), NEMO-PISCES (IPSL) (Aumont et al., 2015), MOM6-COBALT (Princeton) (Liao et al., 2020), MRI-ESM2-2 (Nakano et al., 2011, Urakawa et al., 2020 and Sakamoto et al., 2023), MICOM-HAMOCC (NorESM-OCv1.2) (Schwinger et al., 2016), NEMO-PlankTOM12 (Wright et al., 2021), CESM-ETHZ (Doney et al., 2009), MPIOM-HAMOCC6 (Lacroix et al., 2021) and ACCESS (CSIRO) (Law et al., 2017).

	Mean			
	1958-2019	**1981-2007**	**1994-2007**	**2000-2019**
Global flux (A-B)	-1.53	-1.70	-1.79	-2.00
		(LQ: -2.2)		(GCB: -2.32 [-3.11; -1.91])
CO_2 atmos (C-B)	-1.63	-1.81.	-1.97	-2.25
		(LQ: -0.43)	(G: -2.6±0.2)	(GCB: -2.44 [-3.17; -2.12])
Climate (A-C)	0.10	0.12	0.18	0.25
		(LQ: 0.27)		(GCB: 0.12 [0.05; 0.20])
Winds (A-F)	0.09	0.10	0.15	0.17
Warming (A-E)	0.03	0.01	0.02	0.09
nat (D-B)	0.09	0.11	0.18	0.26
			(G: 0.4±0.2)	
ant ((A-C)-(D-B))	0.01	0.00	-0.00	-0.01
	Trend			
	1958-2019	**1981-2007**	**1994-2007**	**2000-2019**
Global flux (A-B)	-0.238	-0.158	-0.219	-0.397
	(GCB: -0.293 [-0.376; -0.249])	(LQ: -0.12)		
CO_2 atmos (C-B)	-0.304	-0.259	-0.356	-0.332
	(GCB: -0.336 [-0.433; -0.280])	(LQ: -0.32)		
Climate (A-C)	0.065	0.101	0.137	-0.65
	(GCB: 0.044 [0.009; 0.079])	(LQ: 0.20)		
Winds (A-F)	0.029	0.089	0.118	-0.113
		(LQ: 0.12)		
Warming (A-E)	0.023	0.006	0.052	0.076
		(LQ: 0.04)		
nat (D-B)	0.072	0.114	0.179	-0.066
ant ((A-C)-(D-B))	-0.006	-0.013	-0.043	0.001